Selective Area Growth of GaN μ-Platelets on Graphene

Jonathan Henriques, Dyhia Tamsaout, Ludovic Largeau, Edmond Cambril, Lucie Valera, Gwénolé Jacopin, Maria Tchernycheva, Jean-Christophe Harmand, Joël Eymery, Christophe Durand

Selective area growth of GaN µ-platelets on graphene

Jonathan Henriques [1], Dyhia Tamsaout[2], Ludovic Largeau[2], Edmond Cambril[2], Lucie Valera[1,3], Gwénolé Jacopin[3], Maria Tchernycheva[2], Jean-Christophe Harmand[2], Joël Eymery[4], Christophe Durand[1*]*

[1] Université Grenoble Alpes, CEA, Grenoble-INP, IRIG, PHELIQS, NPSC, 38000 Grenoble, France

[2] Centre de Nanoscience et Nanotechnologie (C2N), CNRS, Université Paris-Saclay, 91120 Palaiseau, France

[3] Université Grenoble Alpes, Grenoble-INP, CNRS, Institut Néel, 38000 Grenoble, France

[4] Université Grenoble Alpes, CEA, IRIG, MEM, NRX, 38000 Grenoble, France

KEYWORDS

SAG, Graphene, GaN, Nucleation, MOVPE, PA-MBE, ELOG

ABSTRACT

We report the selective area growth of N-polar GaN μ-platelets on graphene by metalorganic vapor-phase epitaxy. In a first step, GaN nanowires grown by selective molecular beam epitaxy on patterned graphene arrays on SiO_2 are used as nucleation seeds. The initial radius of the graphene patches results in different optical and crystalline quality of the GaN μ-platelets due to different coalescence mechanisms. The use of large graphene patches (250 nm) with significant number of nanowires seeds promotes the growth selectivity on patterned graphene at the expense of the structural quality (presence of voids, stacking faults, dislocations, and inversion domains). On the contrary, the use of smaller patches (65 nm) allows to grow μ-platelets from a very limited seed number (< 3 nanowires) with a significantly reduced number of extended defects. These observations have been directly related to optical measurements by cathodoluminescence and high-resolution transmission electronic microscopy observations performed on the same μ-platelets for the different graphene patch radii (65, 90, 250 nm). The formation of defects is discussed and supported by nucleation, intra- and inter-coalescence mechanisms.

INTRODUCTION

Recently, two-dimensional (2D) materials used for layer transfer have attracted attention due to their weak van der Waals bonds. Especially, the epitaxy of GaN on graphene has been the subject of intensive research in two different approaches: the graphene is either transferred to standard crystalline substrates to promote a so-called remote epitaxy[1–3] or transferred on host substrates without epitaxial matching to induce direct van der Waals epitaxy.[4] III-N semiconductor growth has been demonstrated on hexagonal boron nitride (h-BN), allowing to perform remote epitaxy of nitride devices, such as µLED display easily detachable and transferable.[5] However, the epitaxy of GaN on 2D materials still remains an issue. Indeed, the presence of van der Waals bonds rules out dangling bonds, making it challenging to directly grow GaN on graphene using metal organic vapor-phase epitaxy (MOVPE) reactor. To address this challenge, several strategies have been explored. One solution involves growing a AlGaN[6] or AlN[7] interfacial layer ; the short diffusion length of Al adatoms favors the nucleation process on 2D materials. Similarly, a seed layer of GaN grown at low temperature (700 °C) has also been demonstrated.[8] Another approach reported by K.Chung *et al.*[4,9] consists in the epitaxial lateral overgrowth (ELOG) of organized GaN microdisks, starting from zinc oxide (ZnO) nanowires (NWs) nucleated on graphene. On the other hand, the direct selective growth of GaN NWs on patterned graphene patches onto silicon dioxide (SiO_2) has been successfully demonstrated through plasma-assisted molecular beam epitaxy (PA-MBE).[10,11] This work opens the possibility to use these GaN NWs (instead of ZnO NWs) as seeds to perform homo-ELOG of GaN µ-platelets, acting as organized nano-templates for the fabrication of µLED arrays with dimensions of the range of 1-10 micrometers. This approach based on 2D materials is a promising technique in comparison of various processes already reported in the literature to fabricate flexible µLED arrays,[12] such as laser lift-off,[13,14] chemical lift-off[15,16] and mechanical lift-off.[17–20] The success of the µLED array transferability can support the development of lightweight flexible GaN-based µLEDs[21] with various applications from the next generation of displays[22,23] to the biomedical field.[24]

In this work, we propose a novel approach combining MBE and MOVPE to achieve the 2-step growth of organized GaN µ-platelets on patterned graphene, as depicted in the Fig. 1. The growth of organized GaN µ-platelets by MOVPE follows the selective MBE growth of GaN NWs on graphene. GaN NWs act as nucleation seeds as described in the schematic of Fig. 1(a). The influence of the graphene pattern geometry (radius and pitch) on the morphology and the structural properties of the GaN µ-platelets will be studied and correlated to the optical properties.

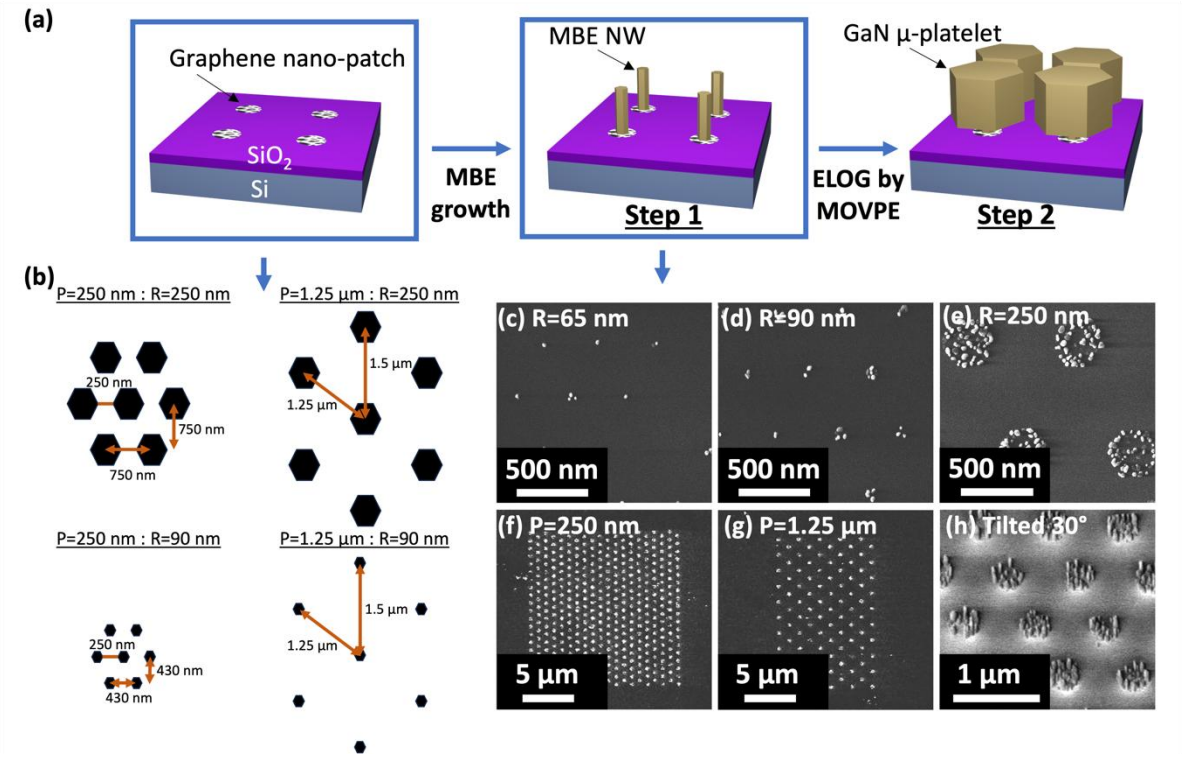

Figure 1. (a) Schematics of the MOVPE growth of µ-platelet from GaN NW seeds on graphene patches. (b) Graphene nano-patch pattern designs. Top-view scanning electron microscopy (SEM) of the initial GaN MBE seeds on different patches of radius R: (c) 65 nm, (d) 90 nm, (e) 250 nm for a pitch P=250 nm, and for different pitches P: (f) 250 nm, (g) 1.25 µm for R=250 nm. (h) 30°-Tilted SEM image of the R=250 nm and P=250 nm pattern showing characteristic sizes of the seeds (100-200 nm length and 20-40 nm diameter).

EXPERIMENTAL METHODS

The graphene patterns, also called nano-patches or dots in the literature, were fabricated using 1 cm^2 commercial polycrystalline graphene grown by chemical vapor deposition (CVD) on a copper foil. The thickness is one monolayer and grain sizes about tens of µm.[25] The graphene is wet-transferred onto 300 nm-thick SiO_2 deposited on Si (001) wafer. The SiO_2 is obtained by thermal oxidation of the Si substrate. The patterning procedure of the nano-patches is obtained by e-beam lithography and O_2-plasma etching as described in ref [10]. Hexagonal shape graphene nano-patches arrays are designed with a radius (R) of 65 to 250 nm (Fig. 1(b-d)) and a pitch distance between the patches (P) of 250 nm to 1.25 µm (Fig. 1(e-f)). The pitch is determined by measuring from the closest edge of the patches for a radius of 250 nm, and center-to-center for 1.25 µm. Then, the sample is transferred into a PA-MBE chamber. The temperature was measured by an optical pyrometer calibrated before each run, by observing the (1 × 1) to (7 × 7) surface reconstruction transition on Si (111), which occurs at 860 °C. Prior to the growth, the substrate was first outgassed at 850°C for 15 min to remove residual impurities from the surface. Afterwards, the substrate was exposed to a Ga flux equivalent to a planar GaN growth rate of 0.62 monolayer/s and to an active N flux corresponding to a N/Ga ratio in the vapor phase of 1.1 in order to grown nominally undoped GaN nanowires. The growth temperature was set at 815°C for a duration of 90 minutes. As shown in Fig. 1(g), selective growth of 150-nm-long N-polar GaN [26] NWs is therefore obtained. According to ref [10], these nanowires are oriented with respect to the underlying graphene layer. The radius determines the number of NWs on the patch. We can get 1-3 NWs only for R=65 nm (Fig. 1(b)), 1-7 NWs for R=90 nm (Fig. 1(c)) and 39 ± 5 for R=250 nm (Fig. 1(d)). It should be noted that these radius values are design parameters and will be used throughout this study. The actual values can be estimated by measuring the radius after the wires have grown. The measured deviations are probably due to the irradiation dose during e-beam lithography and the dry etching during O_2 plasma. For R=250, 90 nm the actual radius is 170 and 50 nm (meaning a pitch of 410 and 330 nm instead of P=250 nm for R=250 and 90 nm). However, as the radius is reduced, the number of NWs is smaller, making the estimate uncertain as the graphene is not directly observable after the growth. This sample with MBE-grown GaN seeds is then transferred into a close-coupled showerhead MOVPE reactor. The MOVPE process includes firstly an annealing at

950 °C for 10 minutes under nitrogen flow to clean the surface, especially the gallium oxide on the MBE NW resulting from the transfer in air. Note that this treatment does not affect significantly the graphene layer as shown in ref [27]. Then, the growth conditions were chosen to promote undoped GaN ELOG on the NW sidewalls with moderate temperature (950 °C) and low pressure (150 mbar) to be in a mass-transport growth regime. Ammonia (NH_3) and triethylgallium (TEGa) were used as precursors to control easily the growth rate with respect to TEGa. The V/III ratio is fixed to 9200 by injecting 50 sccm (7.28 µmol/min) and 1500 sccm (67 mmol/min) flux of TEGa and NH_3 respectively. The growth time is set to 450 s to define the surface coverage by the µ-platelets.

RESULTS AND DISCUSSION

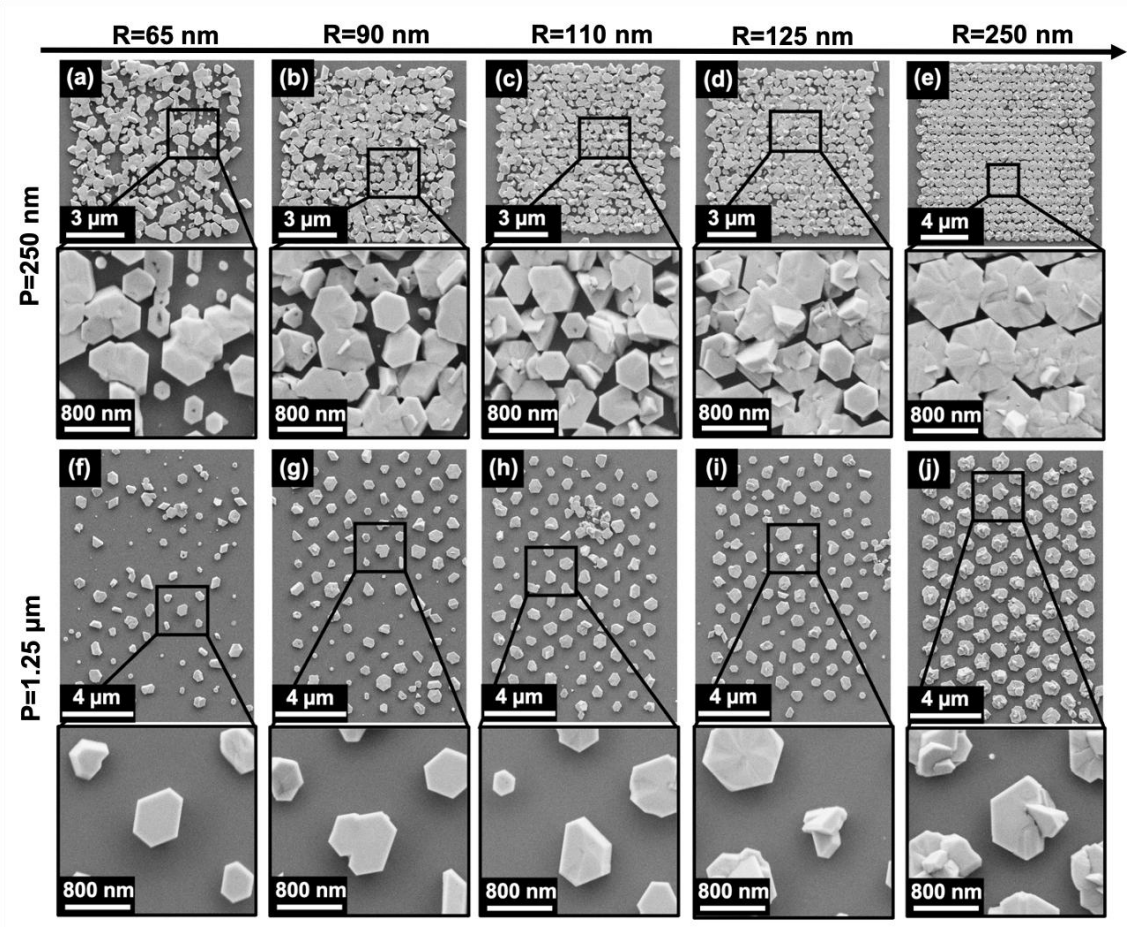

Figure 2. Two magnifications top-view SEM image of the MOVPE lateral growth for P= 250 nm pitch and different R radius of (a) 65 nm, (b) 90 nm (c) 110 nm (d) 125 nm (e) 250 nm. Same view for P=1.25 µm pitch and R radius: (f) 65 nm, (g) 90 nm, (h) 110 nm (i) 125 nm (j) 250 nm.

Scanning electron microscopy (SEM) is performed to study the growth mechanisms involved in this process. Fig. 2(a-j) shows top views of the surface morphology with two magnifications for several graphene patterns with R=65, 90, 110, 125, 250 nm and P =1.25, 0.25 µm. Lateral growth is evidenced by comparison with Figure 1. However, this ELOG is not uniform. Considering first the largest pitch P=1.25 µm in Fig. 2(f-j), the density of overgrowth sites is considerately impacted by the graphene patch radius R. Indeed, for the smaller patch radius (Fig. 2(f)), no overgrowth is observed at specific sites indicating that nucleation is not homogeneous. This is to be related to the fact that when R decreases from 250 to 65 nm, the initial number of MBE GaN NWs is significantly reduced,

from about 40 to only 1-2 NWs. It is difficult to conclude at this point if this is related to a stochastic and therefore heterogeneous nucleation on the NW array (which also presents non-uniformity) or to the lateral NW surface cleaning that has to be improved. The stochastic regime could be attributed to a high growth temperature [28] and to the decreased area available for nucleation at the graphene patches with a small number of seed NWs. Conversely, overgrowth is observed on all patches of 250 nm radius which contain initially a large number of NWs (Fig. 2(j)). This probably increases the nucleation probability. In the case of the largest patch radius, the high probability of regrowth favors a quasi-simultaneous growth leading to µ-platelets with approximately the same area. For the smallest dot radius, the inhomogeneity of µ-platelet size and shape is explained by an asynchronous start of regrowth due to the fewer MBE NWs. Even though the use of a large radius leads to a better homogeneity of GaN overgrowth, the presence of multiple NWs can also lead to morphological defects, since the NWs act as independent nucleation centers which, at some point, lead to a radial coalescence of several GaN nanocrystals. This coalescence at each single graphene patch (referred to as intra-coalescence in the following sections) can induce the formation of extended defects such as stacking faults, dislocations, and grain boundaries.[29–31] Moreover, decreasing the pitch down to 250 nm (Fig. 2(a-d)) yields a noticeable effect on overgrowth. Especially for lower R values (e.g., R=65 nm in Fig. 2(a)), the periodicity of the initial pattern is difficult to identify after overgrowth. This can be explained by an asynchronous start of regrowth from one patch to another. Growth competition between the large and small objects may follow, considering the two diffusion paths in MOVPE (surface and gas phase) to feed the growth. This phenomenon can amplify the size dispersion of the µ-platelets which relates initially to their asynchronous growth start. After a certain growth time, the largest µ-platelets exceed the pitch distance. This effect results in µ-platelet merging from different patches and will be called inter-coalescence. This is mostly observed for small radius and pitch. This inter-coalescence will also induce local strains between the patches because their crystalline orientations are not perfectly aligned (they follow the orientation of the MBE-grown NWs which is determined by that of the transferred graphene). For the chosen growth time of 450s, well-arranged

hexagonal shaped µ-platelets are only observed for an array corresponding to R=250 nm and P=250 nm (Fig. 2(e)). In this case, some µ-platelet edges are just in contact with their neighbours. For this patch geometry, the µ-platelets show a quite regular hexagonal shape in comparison to other configurations, possibly due to a lower growth rate [32] that favours the formation of *m*-plane facets. This section demonstrates the MOVPE regrowth on organized GaN NWs that are epitaxially grown on graphene by MBE. We have shown that the pattern design has a strong impact on the nucleation probability and on the lateral regrowth morphology due to intra- and inter-coalescence phenomena. To evaluate their respective impacts on the optical properties, cathodoluminescence (CL) measurements were performed.

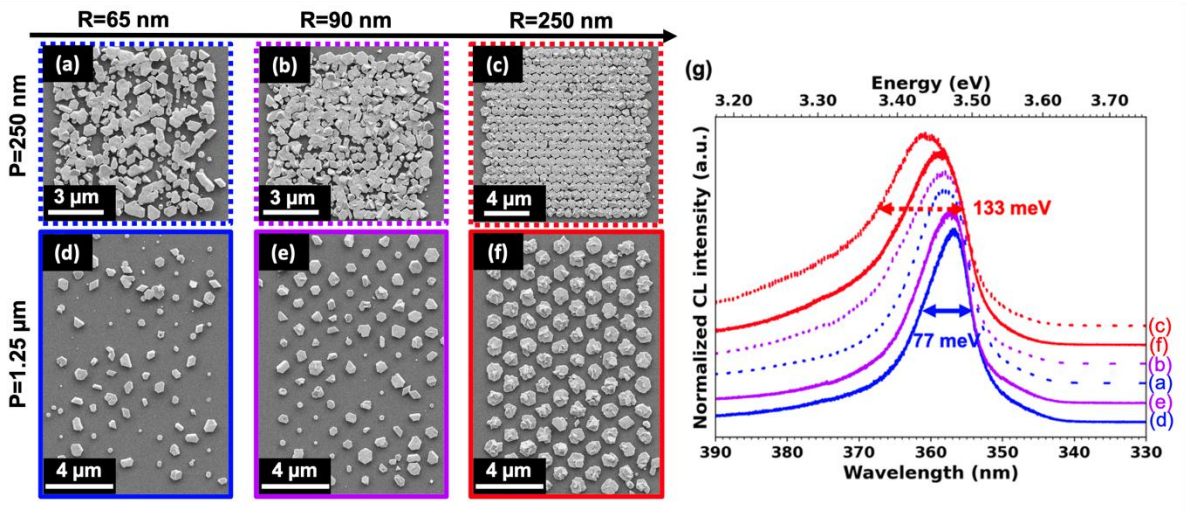

Figure 3. Top-view SEM image of the MOVPE GaN lateral growth on 250 nm graphene pitch for R: (a) 65 nm, (b) 90 nm (c) 250 nm and on 1.25 µm pitch for R: (d) 65 nm, (e) 90 nm, (f) 250 nm. Each SEM image is associated with its CL spectra (g) taken at 5 K.

CL measurements combining hyperspectral mapping and spectral measurements are carried out at 5 K to investigate the optical properties of the µ-platelets, as a function of the pattern design and consequently of the coalescence defects. The acceleration voltage is set at 5 kV. At such voltage, the penetration depth of electrons is about 200 nm in GaN. The CL signal is then collected thanks to a parabolic mirror and analyzed by a spectrometer coupled to a charge-coupled device (CCD). Fig. 3(a-

f) shows the SEM images of six different patterns and their corresponding normalized CL spectra given in Fig. 3(g). Each CL signal reflects the integrated luminescence emitted by all the µ-platelets of the SEM zones. We can note a dependence of both the luminescence peak positions and their full widths at half maximum (FWHM) on the array geometry. In the case of R=250 nm and P=250 nm (Fig. 3(c)), the peak exhibits the largest FWHM with a value of 133 meV and also the largest red-shift leading to an emission at 3.436 eV. Generally, the predominant peaks observed in GaN are the excitons bound to neutral donor (D^0X_A) and the free exciton (X_A), positioned at 3.471 and 3.478 eV, respectively [33]. This variation of the emission wavelength may be explained by the presence of strain[34] and/or additional contributions emitting at lower energy levels related to defects (such as basal stacking faults (BSFs) I_1, I_2, E radiating at 3.41[35], 3.32[36] to 3.38[37] and 3.29[38] respectively). Here, the degraded optical quality can be attributed to intra- and inter-coalescence defects caused by both the high number of NWs in each graphene patch and the short spacing, resulting in overlapping spectra of defective individual µ-platelets. As the pitch is increased to 1.25 µm (Fig. 3(f)), we avoid the inter-coalescence between µ-platelets and the FWHM is reduced to 112 meV with a slight increase in emission energy at 3.457 eV. Considering that the only difference is the pitch value, this increase in energy can then be directly linked to the absence of certain structural defects and strain in this case. The optical emission is further improved when R is reduced to 90 nm (for P=250 nm), as shown in Figure 3(b). We measure a FWHM of 108 meV with an emission taking place at 3.463 eV. Significant improvement in optical properties is also reached by increasing the pitch (Figure 3(e)), again because of elimination of any inter-platelet coalescence effects. In this case, the FWHM is reduced to 82 meV, and the emission energy at 3.471 eV is achieved, which is close to the expected value for bulk GaN. This result can be explained by the reduction of defects due to the limited number of NWs in a nano-patch. Indeed, the best emission properties (FWHM down to 77 meV and emission energy at 3.476 eV) are obtained for the pattern with R=65 nm and P=1.25 µm (Figure 4(d)), where only 1-2 NWs per patch were observed before regrowth. This result tends to demonstrate that to benefit from the method proposed in this paper, each graphene patch must initially contain a

small number of NW seeds (ideally one per patch), and inter-patch coalescence must be avoided by controlling the growth time. To better understand the origin of the large and shifted CL emission peak of large patches, we then performed hyperspectral mappings to analyze the internal inhomogeneity within the μ-platelets.

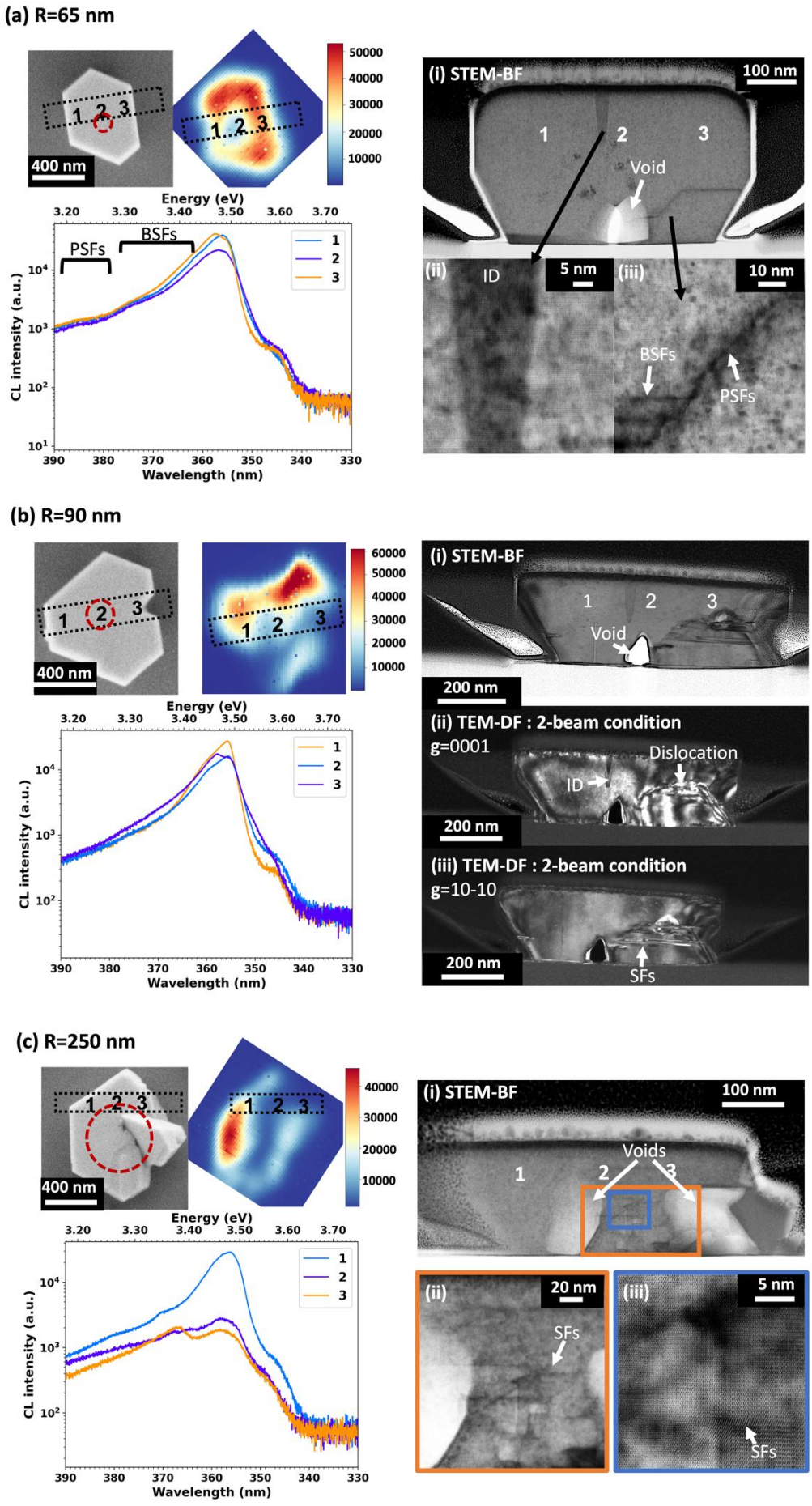
(a) R=65 nm
400 nm
1 2 3
50000
40000
30000
20000
10000
Energy (eV)
3.20 3.30 3.40 3.50 3.60 3.70
PSFs
BSFs
CL intensity (a.u.)
Wavelength (nm)
390 380 370 360 350 340 330
(i) STEM-BF
100 nm
Void
(ii)
ID
5 nm
(iii)
10 nm
BSFs
PSFs
(b) R=90 nm
60000
50000
40000
30000
20000
10000
(i) STEM-BF
Void
200 nm
(ii) TEM-DF : 2-beam condition
g=0001
Dislocation
ID
(iii) TEM-DF : 2-beam condition
g=10-10
SFs
(c) R=250 nm
(i) STEM-BF
100 nm
Voids
20 nm
5 nm

Figure 4. GaN µ-platelet of P=1.25 µm pitch and R=: (a) 65 nm, (b) 90 nm, and (c) 250 nm. Each panel includes: top-view SEM images with their respective CL spectra associated to the number displaying on the hyperspectral mapping. Each µ-platelets is associated with its cross-section STEM images taken along the a-axis zone in bright field mode ((a-i)(b-i)(c-i)). TEM dark field mode is also reported in (b) along the c-axis (b-ii) and a-axis (b-iii). The voids, dislocations, prismatic (PSFs) and basal (BSFS) stacking faults (SFs) are highligted in the TEM and STEM images.

Correlation between optical emission properties and structural defects can be obtained by performing cathodoluminescence measurements, high-resolution transmission electron microscopy (HRTEM) and high-resolution scanning transmission electron microscopy (HRSTEM) observations on the same single GaN µ-platelet. We selected non-overlapping µ-platelets from arrays with P=1.25 µm and collected hyperspectral CL map on µ-platelets with R=65, 90, 250 nm (figure 4). Following CL measurements, these platelets were thinned by focused ion beam (FIB) for HRTEM observation. The exact location of the TEM lamellae prepared by FIB is indicated by the dotted rectangles drawn on SEM top views (figure 4). The thickness of TEM lamellae was about 100 nm. The TEM observations have been obtained using a ThermoFisher 200 Titan probe aberration corrected TEM/STEM. Two types of TEM imaging conditions have been used. Bright Field Scanning Transmission Electron Microscopy (BF-STEM) allows to collect images down to the atomic scale while maintaining a contrast sensitive to strains induced by extended defects. Dark field (DF) TEM images collected in a 2-beam condition allows to image extended defects with lattice shift parallel to the reciprocal space vector **g**.

An inverted pyramidal morphology is observed for R=65 and 90 nm. The edges correspond to *r*-planes which form an angle of 62° with the *c*-plane. This surface is relatively stable and is commonly observed in nitride growth.[39] This is consistent with ELOG on N-polar NWs which tends to develop the N-polarity, leading to upside-down pyramids combining inclined *r*-facets and vertical *m*-facets.[40] Figure 4(a) shows that the CL spectra recorded from three zones along the platelet diameter are similar in the case of a small 65 nm-patch. The emission is dominated by a broad signal around 3.48 eV related to the GaN near band edge (NBE) emission, but additional contributions are also visible at

3.22 eV and 3.33 eV. These low-energy peaks have been identified in the literature as the signature of GaN prismatic (PSFs) and basal stacking faults (BSFs), respectively.[41] The PSFs are assigned to the intersection of BSFs and a partial dislocation.[42] The HR BF-STEM images confirm the presence of BSFs attached with a PSFs in Fig. 4(a-iii), which subsequently evolve into BSFs to reach the *r*-plane surface. Furthermore, the µ-platelet exhibits in Fig. 4(a-ii) a change of contrast just above the void that can be attributed to an inversion domain (ID).[43] This Ga-polar phase is probably contributing to the broadening of the NBE emission at 3.45 eV.[44] This ID feature also appears for R=90 nm. The associated shift in lattice lying along the *c*-direction is clearly visible in a 2-beam DFTEM images using **g**=0001. It has been demonstrated that the Ga-polarity NBE emits less than the N-polarity due to preferential dopant and impurity incorporation. Therefore, this ID may play a role in reducing the intensity at the center of the µ-platelets hyperspectral mapping in Fig 4(a-b).[45,46] Additionally, the top-view SEM image reveals the merging of multiple hexagons, suggesting the coalescence of inverted pyramids. The TEM image (Fig. 4(b-ii)) shows an inter-grain dislocation at the right side of the void, likely resulting from intra-coalescence among these crystals. The hyperspectral map and the spectrum at this specific zone (zone 3) reveal a clear decrease in intensity associated to non-radiative defects, whereas a slight increase is observed in the region near 3.3 eV, consistent with the presence of numerous BSFs, as revealed by the 2-beam DFTEM image using **g**=10-10 (see Fig. 4(b-iii)). In the case of the larger diameter R=250 nm, the intra-coalescence phenomenon is enhanced due to the initial presence of multiple GaN NWs. They promote the formation of larger voids and a higher density of extended defects (such as SFs). A decrease in CL intensity of the hyperspectral mapping is measured at the center for R=250 nm sample. The lateral extent of this decrease correlates with the presence of large voids observed inside the platelet and close to their center. These voids not only correspond to a reduced volume of GaN but also introduce internal surfaces. Both are very likely to contribute to the decrease of luminescence intensity. As shown in the zone 2 of Fig. 4(c-ii), the central region between the two voids exhibits numerous defects, primarily basal stacking faults (BSFs) and the CL peak associated with BSFs (3.38 eV) dominates the GaN NBE emission. The defects

summarized as a function of the graphene patch radius are presented in Table 1. In addition, a peak around 3.58 eV is observed in most of the spectra. This peak results from strain, since its emission is located at a higher energy than the NBE of GaN. The origin of this strain is unclear and could come from multiple sources, such as dislocations, cubic inclusions and grain boundaries.

Graphene radius (R)	**Initial Number of NWs**	**Defects observed on μ-platelets**
65 nm	1-2	One small void ID Few PSFs and BSFs
90 nm	1-7	One small void Dislocations Many BSFs ID
250 nm	39 ± 5	Two large voids Many PSFs and BSFs

Table 1. Summary of the defects observed in μ-platelets by STEM and TEM as a function of the graphene patch radius.

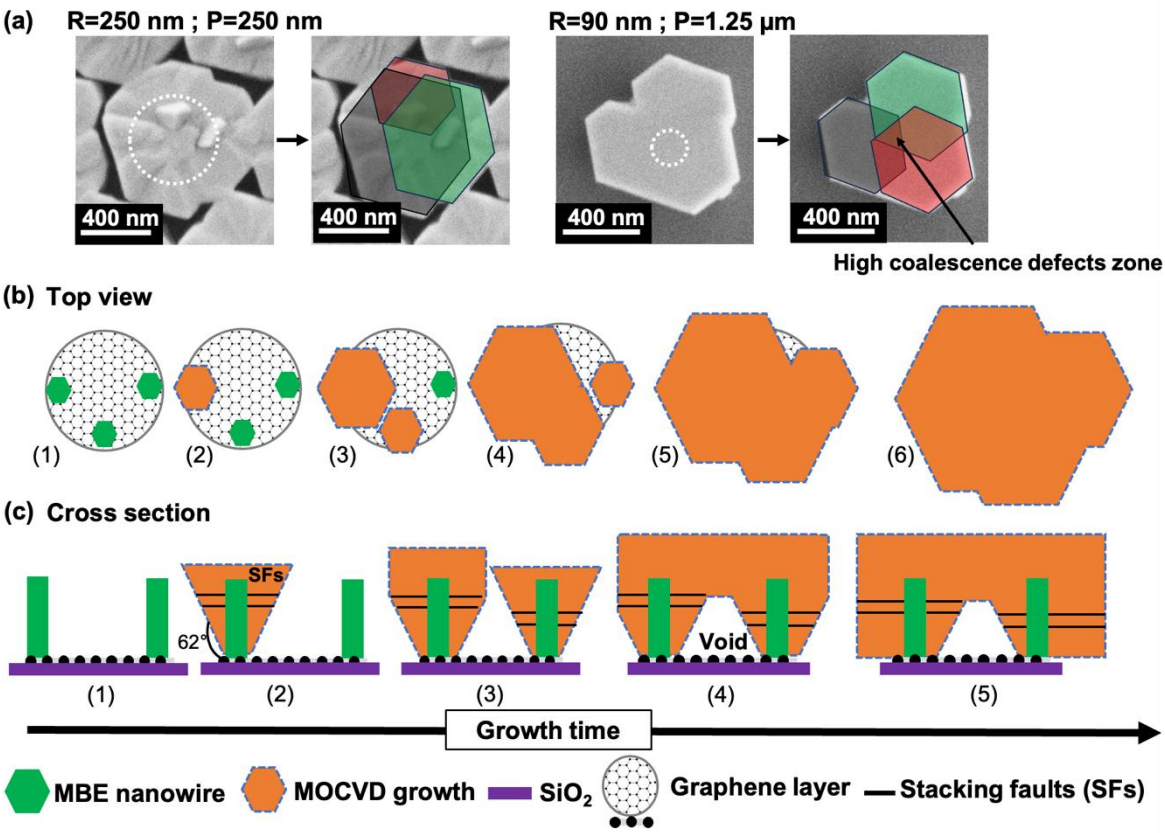

Figure 5. (a) Top-view SEM images of R=250 nm/P=250 nm and R=90 nm/P=1.25 µm graphene patterns having multiple hexagonal crystals embedded in a µ-platelet. Schematic procces of the growth of µ-platelets in (b) top-view and (c) cross-section.

To summarize our experimental observations, we demonstrated that the µ-platelets exhibit significantly different morphological, optical and structural characteristics depending on the pattern geometry. Fig. 5(a) shows top-view SEM images of two different patches. Their morphologies can be described by several interconnected non regular hexagonal crystals with *m*-plane sidewall facets (commonly observed in GaN islands and nanostructures).[47] The general orientation of these hexagons is determined by the epitaxy on graphene and will follow the disorientations introduced by the grains of polycrystalline graphene[10]. To explain the experimental observations, we propose in Figure 5(b-c) a schematic of the MOVPE regrowth process on the MBE NWs for the top- and cross-section views. Note first that MBE NWs grow preferentially at the edge of the graphene patch, as depicted in Figure 1 and Figure 5(b-c). During the initial stages of MOVPE growth, two effects

increase the size distribution of the objects: re-growth on different sites may not start at the same time and growth rate may vary from site to site due to diffusion at the surface and in the gas phase which is sensitive to the presence of already formed crystals. In the literature, it has been proposed to force simultaneous nucleation on different sites using a two-step growth process, initiating the growth at low temperature to decrease the diffusion length (for example 950°C/1040°C).[40] With growth time, multiple crystallites of different sizes form and then coalesce leading to a morphology that corresponds to the SEM image shown in Figure 5(a). The top views are complemented by cross-section observations. We observe that the µ-platelets have an inverted pyramidal shape with *r*- and *m*-planes facets as schematized in step (2) and (3) of the Fig 5(c). It has been demonstrated in the literature that GaN pyramidal shape induce BSFs that can extend laterally into the crystal to end at *r*-plane facets as already observed in Ref [42]. In an intermediate stage and when two nucleation centers are close to each other, the coalescence of these 3D-objects (Fig. 5(c): step (3) and (4)) results in the formation of a triangular void, as observed in TEM. This void could promote the formation of an ID linked to interfacial defects and the possibility of having inter-grain dislocations that can be mixed with BSFs. Note that these defects are buried under the surface, and therefore they do not degrade too much the crystalline quality of the top of the µ-platelets. Focusing on the overall morphology of the µ-platelet, the rapid growth along the *r*-plane promotes the gradual development of *m*-plane facets over time. This was observed after a growth period of 450 seconds. Finally, the *r*-plane gradually disappears to the benefit of the *m*-plane area, facilitating full lateral expansion without the occurrence of additional defects.

CONCLUSIONS

In summary, we use GaN NWs selectively grown by MBE on patterned graphene to perform the overgrowth of organized GaN µ-platelets by MOVPE. It has been demonstrated that the pattern geometry of graphene and the density of NW seeds strongly influences the optical and crystalline

quality of the μ-platelets due to intra- and inter-coalescence of the different nucleation NW sites. The use of a large number of NWs efficiently promotes the selective MOVPE growth of μ-platelets for a temperature of 950°C. Nevertheless, intra-coalescence results in the formation of voids and various extended defects, including stacking faults, dislocations, and domain inversions. These defects significantly impact optical emission properties, either by diminishing intensity due to reduced volume of material and carrier recombination on non-radiative centers or by adding additional emission peaks between 3.2 and 3.4 eV due to the presence of stacking faults. The growth on a very limited number of NWs (ideally a single GaN NW) is the better solution to reduce significantly the defect density.

AUTHOR INFORMATION

Corresponding Author

Jonathan Henriques - jonathan.henriques@cea.fr

Christophe Durand - christophe.durand@cea.fr

Author Contributions

J.H performed the MOVPE growths, CL measurements, SEM observations, the analyses and took an active part in the writing of this manuscript with support from supervisors C.D. and J.E.; D.T. and E.C. performed the preparation of the patterned substrates; D.T. performed the MBE growths; L.L. performed the FIB preparations and TEM analyses. L.V. and G.J. took part in the CL measurements. C.D., M.T. and J-C. H involved in the project management and fundings. All authors have participated to the correction of the manuscript and have given approval to the final version of the manuscript.

Funding Sources

This research was funded by the French National Research Agency in the framework of the project FLAGG ANR-21-CE24-0017-01. This work was partly supported by the French RENATECH network (MBE growth, FIB preparation, TEM observations).

Notes

The authors declare no competing financial interest.

ACKNOWLEDGMENTS

The authors thank J. Dussaud for his work on the MOVPE setup, Fabrice Donatini (from Néel institute) for his help with cathodoluminescence measurements and the PFNC of CEA Grenoble (SEM observations).

REFERENCES

(1) Han, X.; Yu, J.; Li, Z.; Wang, X.; Hao, Z.; Luo, Y.; Sun, C.; Han, Y.; Xiong, B.; Wang, J.; Li, H.; Zhang, Y.; Duan, B.; Ning, J.; Wu, H.; Wang, L. Remote Epitaxy and Exfoliation of GaN via Graphene. *ACS Appl. Electron. Mater.* **2022**, *4* (11), 5326–5332. https://doi.org/10.1021/acsaelm.2c00997.

(2) Kim, Y.; Cruz, S. S.; Lee, K.; Alawode, B. O.; Choi, C.; Song, Y.; Johnson, J. M.; Heidelberger, C.; Kong, W.; Choi, S.; Qiao, K.; Almansouri, I.; Fitzgerald, E. A.; Kong, J.; Kolpak, A. M.; Hwang, J.; Kim, J. Remote Epitaxy through Graphene Enables Two-Dimensional Material-Based Layer Transfer. *Nature* **2017**, *544* (7650), 340–343. https://doi.org/10.1038/nature22053.

(3) Kim, J.; Bayram, C.; Park, H.; Cheng, C.-W.; Dimitrakopoulos, C.; Ott, J. A.; Reuter, K. B.; Bedell, S. W.; Sadana, D. K. Principle of Direct van Der Waals Epitaxy of Single-Crystalline Films on Epitaxial Graphene. *Nat. Commun.* **2014**, *5* (1), 4836. https://doi.org/10.1038/ncomms5836.

(4) Singh, A. K.; Ahn, K.; Yoo, D.; Lee, S.; Ali, A.; Yi, G.-C.; Chung, K. Van Der Waals Integration of GaN Light-Emitting Diode Arrays on Foreign Graphene Films Using Semiconductor/Graphene Heterostructures. *NPG Asia Mater.* **2022**, *14* (1), 57. https://doi.org/10.1038/s41427-022-00403-6.

(5) Shin, J.; Kim, H.; Sundaram, S.; Jeong, J.; Park, B.-I.; Chang, C. S.; Choi, J.; Kim, T.; Saravanapavanantham, M.; Lu, K.; Kim, S.; Suh, J. M.; Kim, K. S.; Song, M.-K.; Liu, Y.; Qiao, K.; Kim, J. H.; Kim, Y.; Kang, J.-H.; Kim, J.; Lee, D.; Lee, J.; Kim, J. S.; Lee, H. E.; Yeon, H.; Kum, H. S.; Bae, S.-H.; Bulovic, V.; Yu, K. J.; Lee, K.; Chung, K.; Hong, Y. J.; Ougazzaden, A.; Kim, J. Vertical Full-Colour Micro-LEDs via 2D Materials-Based Layer Transfer. *Nature* **2023**, *614* (7946), 81–87. https://doi.org/10.1038/s41586-022-05612-1.

(6) Sundaram, S.; Vuong, P.; Mballo, A.; Ayari, T.; Karrakchou, S.; Patriarche, G.; Voss, P. L.; Salvestrini, J. P.; Ougazzaden, A. MOVPE of GaN-Based Mixed Dimensional Heterostructures on

Wafer-Scale Layered 2D Hexagonal Boron Nitride—A Key Enabler of III-Nitride Flexible Optoelectronics. *APL Mater.* **2021**, *9* (6), 061101. https://doi.org/10.1063/5.0049306.

(7) Liudi Mulyo, A.; Mukherjee, A.; Høiaas, I. M.; Ahtapodov, L.; Nilsen, T. A.; Toftevaag, H. H.; Vullum, P. E.; Kishino, K.; Weman, H.; Fimland, B.-O. Graphene-Based Transparent Conducting Substrates for GaN/AlGaN Nanocolumn Flip-Chip Ultraviolet Light-Emitting Diodes. *ACS Appl. Nano Mater.* **2021**, *4* (9), 9653–9664. https://doi.org/10.1021/acsanm.1c02050.

(8) Badokas, K.; Kadys, A.; Mickevičius, J.; Ignatjev, I.; Skapas, M.; Stanionytė, S.; Radiunas, E.; Juška, G.; Malinauskas, T. Remote Epitaxy of GaN via Graphene on GaN/Sapphire Templates. *J. Phys. Appl. Phys.* **2021**, *54* (20), 205103. https://doi.org/10.1088/1361-6463/abe500.

(9) Baek, H.; Lee, C.-H.; Chung, K.; Yi, G.-C. Epitaxial GaN Microdisk Lasers Grown on Graphene Microdots. *Nano Lett.* **2013**, *13* (6), 2782–2785. https://doi.org/10.1021/nl401011x.

(10) Morassi, M.; Guan, N.; Dubrovskii, V. G.; Berdnikov, Y.; Barbier, C.; Mancini, L.; Largeau, L.; Babichev, A. V.; Kumaresan, V.; Julien, F. H.; Travers, L.; Gogneau, N.; Harmand, J.-C.; Tchernycheva, M. Selective Area Growth of GaN Nanowires on Graphene Nanodots. *Cryst. Growth Des.* **2020**, *20* (2), 552–559. https://doi.org/10.1021/acs.cgd.9b00556.

(11) Kumaresan, V.; Largeau, L.; Madouri, A.; Glas, F.; Zhang, H.; Oehler, F.; Cavanna, A.; Babichev, A.; Travers, L.; Gogneau, N.; Tchernycheva, M.; Harmand, J.-C. Epitaxy of GaN Nanowires on Graphene. *Nano Lett.* **2016**, *16* (8), 4895–4902. https://doi.org/10.1021/acs.nanolett.6b01453.

(12) Bosch, J.; Durand, C.; Alloing, B.; Tchernycheva, M. Fabrication Strategies of Flexible Light Sources Based on Micro/Nano III-Nitride LEDs. *J. Inf. Disp.* **2024**, *25* (1), 61–73. https://doi.org/10.1080/15980316.2024.2310638.

(13) Hu, L.; Choi, J.; Hwangbo, S.; Kwon, D.-H.; Jang, B.; Ji, S.; Kim, J.-H.; Han, S.-K.; Ahn, J.-H. Flexible Micro-LED Display and Its Application in Gbps Multi-Channel Visible Light Communication. *Npj Flex. Electron.* **2022**, *6* (1), 100. https://doi.org/10.1038/s41528-022-00234-z.

(14) Asad, M.; Li, Q.; Sachdev, M.; Wong, W. S. Thermal and Optical Properties of High-Density GaN Micro-LED Arrays on Flexible Substrates. *Nano Energy* **2020**, *73*, 104724. https://doi.org/10.1016/j.nanoen.2020.104724.

(15) Lee, C.; Kim, Y.; Hong, Y. J.; Jeon, S.; Bae, S.; Hong, B. H.; Yi, G. Flexible Inorganic Nanostructure Light-Emitting Diodes Fabricated on Graphene Films. *Adv. Mater.* **2011**, *23* (40), 4614–4619. https://doi.org/10.1002/adma.201102407.

(16) Chen, J.; Wang, J.; Ji, K.; Jiang, B.; Cui, X.; Sha, W.; Wang, B.; Dai, X.; Hua, Q.; Wan, L.; Hu, W. Flexible, Stretchable, and Transparent InGaN/GaN Multiple Quantum Wells/Polyacrylamide Hydrogel-Based Light Emitting Diodes. *Nano Res.* **2022**, *15* (6), 5492–5499. https://doi.org/10.1007/s12274-022-4170-4.

(17) Dai, X.; Messanvi, A.; Zhang, H.; Durand, C.; Eymery, J.; Bougerol, C.; Julien, F. H.; Tchernycheva, M. Flexible Light-Emitting Diodes Based on Vertical Nitride Nanowires. *Nano Lett.* **2015**, *15* (10), 6958–6964. https://doi.org/10.1021/acs.nanolett.5b02900.

(18) Guan, N.; Dai, X.; Messanvi, A.; Zhang, H.; Yan, J.; Gautier, E.; Bougerol, C.; Julien, F. H.; Durand, C.; Eymery, J.; Tchernycheva, M. Flexible White Light Emitting Diodes Based on Nitride Nanowires and Nanophosphors. *ACS Photonics* **2016**, *3* (4), 597–603. https://doi.org/10.1021/acsphotonics.5b00696.

(19) Park, J.-B.; Lee, K. H.; Han, S. H.; Chung, T. H.; Kwak, M. K.; Rho, H.; Jeong, T.; Ha, J.-S. Stable and Efficient Transfer-Printing Including Repair Using a GaN-Based Microscale Light-Emitting Diode Array for Deformable Displays. *Sci. Rep.* **2019**, *9* (1), 11551. https://doi.org/10.1038/s41598-019-47449-1.

(20) Jeong, J.; Wang, Q.; Cha, J.; Jin, D. K.; Shin, D. H.; Kwon, S.; Kang, B. K.; Jang, J. H.; Yang, W. S.; Choi, Y. S.; Yoo, J.; Kim, J. K.; Lee, C.-H.; Lee, S. W.; Zakhidov, A.; Hong, S.; Kim, M. J.; Hong, Y. J. Remote Heteroepitaxy of GaN Microrod Heterostructures for Deformable Light-Emitting Diodes and Wafer Recycle. *Sci. Adv.* **2020**, *6* (23), eaaz5180. https://doi.org/10.1126/sciadv.aaz5180.

(21) Fabunmi, T. G.; Lee, S.; Kim, H. I.; Yoo, D.; Lee, J.; Kim, I.; Ali, A.; Jang, D.; Lee, S.; Lee, C.; Kim, M.; Yi, G.-C. Single-Crystalline GaN Microdisk Arrays Grown on Graphene for Flexible Micro-LED Application. *Nanotechnology* **2024**, *35* (8), 085603. https://doi.org/10.1088/1361-6528/ad0e92.

(22) Anwar, A. R.; Sajjad, M. T.; Johar, M. A.; Hernández-Gutiérrez, C. A.; Usman, M.; Łepkowski, S. P. Recent Progress in Micro-LED-Based Display Technologies. *Laser Photonics Rev.* **2022**, *16* (6), 2100427. https://doi.org/10.1002/lpor.202100427.

(23) Chen, D.; Chen, Y.-C.; Zeng, G.; Zhang, D. W.; Lu, H.-L. Integration Technology of Micro-LED for Next-Generation Display. *Research* **2023**, *6*, 0047. https://doi.org/10.34133/research.0047.

(24) Goßler, C.; Bierbrauer, C.; Moser, R.; Kunzer, M.; Holc, K.; Pletschen, W.; Köhler, K.; Wagner, J.; Schwaerzle, M.; Ruther, P.; Paul, O.; Neef, J.; Keppeler, D.; Hoch, G.; Moser, T.; Schwarz, U. T. GaN-Based Micro-LED Arrays on Flexible Substrates for Optical Cochlear Implants. *J. Phys. Appl. Phys.* **2014**, *47* (20), 205401. https://doi.org/10.1088/0022-3727/47/20/205401.

(25) Barbier, C.; Largeau, L.; Gogneau, N.; Travers, L.; David, C.; Madouri, A.; Tamsaout, D.; Girard, J.-C.; Rodary, G.; Montigaud, H.; Durand, C.; Tchernycheva, M.; Glas, F.; Harmand, J.-C. What Triggers Epitaxial Growth of GaN on Graphene? *Cryst. Growth Des.* **2023**, *23* (9), 6517–6525. https://doi.org/10.1021/acs.cgd.3c00481.

(26) Pavlov, A.; Mozharov, A.; Berdnikov, Y.; Barbier, C.; Harmand, J.-C.; Tchernycheva, M.; Polozkov, R.; Mukhin, I. Crystal Polarity Discrimination in GaN Nanowires on Graphene. *J. Mater. Chem. C* **2021**, *9* (31), 9997–10004. https://doi.org/10.1039/D1TC02710G.

(27) Kwak, H.-M.; Kim, J.; Lee, J.-S.; Kim, J.; Baik, J.; Choi, S.-Y.; Shin, S.; Kim, J.-S.; Mun, S.-H.; Kim, K.-P.; Oh, S. H.; Lee, D.-S. 2D-Material-Assisted GaN Growth on GaN Template by MOCVD and Its Exfoliation Strategy. *ACS Appl. Mater. Interfaces* **2023**, *15* (50), 59025–59036. https://doi.org/10.1021/acsami.3c14076.

(28) Li, S.; Wang, X.; Mohajerani, M. S.; Fündling, S.; Erenburg, M.; Wei, J.; Wehmann, H.-H.; Waag, A.; Mandl, M.; Bergbauer, W.; Strassburg, M. Dependence of N-Polar GaN Rod Morphology on Growth Parameters during Selective Area Growth by MOVPE. *J. Cryst. Growth* **2013**, *364*, 149–154.

https://doi.org/10.1016/j.jcrysgro.2012.11.027.

(29) Huang, C.-N.; Shields, P. A.; Allsopp, D. W. E.; Trampert, A. Coalescence-Induced Planar Defects in GaN Layers Grown on Ordered Arrays of Nanorods by Metal–Organic Vapour Phase Epitaxy. *Philos. Mag.* **2013**, *93* (23), 3154–3166. https://doi.org/10.1080/14786435.2013.805272.

(30) Shields, P.; Liu, C.; Šatka, A.; Trampert, A.; Zúñiga-Pérez, J.; Alloing, B.; Haško, D.; Uherek, F.; Wang, W.; Causa, F.; Allsopp, D. Nanopendeo Coalescence Overgrowth of GaN on Etched Nanorod Array. *Phys. Status Solidi C* **2011**, *8* (7–8), 2334–2336. https://doi.org/10.1002/pssc.201000996.

(31) Dagher, R.; De Mierry, P.; Alloing, B.; Brändli, V.; Portail, M.; Damilano, B.; Mante, N.; Bernier, N.; Gergaud, P.; Cottat, M.; Gourgon, C.; Perez, J. Z.; Feuillet, G. Pendeo-Epitaxy of GaN on SOI Nano-Pillars: Freestanding and Relaxed GaN Platelets on Silicon with a Reduced Dislocation Density. *J. Cryst. Growth* **2019**, *526*, 125235. https://doi.org/10.1016/j.jcrysgro.2019.125235.

(32) Coulon, P.; Alloing, B.; Brändli, V.; Lefebvre, D.; Chenot, S.; Zúñiga-Pérez, J. Selective Area Growth of Ga-polar GaN Nanowire Arrays by Continuous-flow MOVPE: A Systematic Study on the Effect of Growth Conditions on the Array Properties. *Phys. Status Solidi B* **2015**, *252* (5), 1096–1103. https://doi.org/10.1002/pssb.201451589.

(33) Reshchikov, M. A.; Morkoç, H. Luminescence Properties of Defects in GaN. *J. Appl. Phys.* **2005**, *97* (6), 061301. https://doi.org/10.1063/1.1868059.

(34) Davydov, V. Yu.; Averkiev, N. S.; Goncharuk, I. N.; Nelson, D. K.; Nikitina, I. P.; Polkovnikov, A. S.; Smirnov, A. N.; Jacobson, M. A.; Semchinova, O. K. Raman and Photoluminescence Studies of Biaxial Strain in GaN Epitaxial Layers Grown on 6H–SiC. *J. Appl. Phys.* **1997**, *82* (10), 5097–5102. https://doi.org/10.1063/1.366310.

(35) Gühne, T.; Bougrioua, Z.; Vennéguès, P.; Leroux, M.; Albrecht, M. Cathodoluminescence Spectroscopy of Epitaxial-Lateral-Overgrown Nonpolar (11-20) and Semipolar (11-22) GaN in Relation to Microstructural Characterization. *J. Appl. Phys.* **2007**, *101* (11), 113101. https://doi.org/10.1063/1.2740361.

(36) Tischer, I.; Feneberg, M.; Schirra, M.; Yacoub, H.; Sauer, R.; Thonke, K.; Wunderer, T.; Scholz, F.; Dieterle, L.; Müller, E.; Gerthsen, D. I 2 Basal Plane Stacking Fault in GaN: Origin of the 3.32 eV Luminescence Band. *Phys. Rev. B* **2011**, *83* (3), 035314. https://doi.org/10.1103/PhysRevB.83.035314.

(37) Chen, J.; Yi, W.; Ito, S.; Sekiguchi, T. Cathodoluminescence Investigation of Stacking Faults and Dislocations in the Edge Part of Seed-Grown *m* -Plane GaN Substrate. *Phys. Status Solidi A* **2021**, *218* (14), 2100175. https://doi.org/10.1002/pssa.202100175.

(38) Lähnemann, J.; Jahn, U.; Brandt, O.; Flissikowski, T.; Dogan, P.; Grahn, H. T. Luminescence Associated with Stacking Faults in GaN. *J. Phys. Appl. Phys.* **2014**, *47* (42), 423001. https://doi.org/10.1088/0022-3727/47/42/423001.

(39) Bi, Z.; Gustafsson, A.; Lenrick, F.; Lindgren, D.; Hultin, O.; Wallenberg, L. R.; Ohlsson, B. J.; Monemar, B.; Samuelson, L. High In-Content InGaN Nano-Pyramids: Tuning Crystal Homogeneity by Optimized Nucleation of GaN Seeds. *J. Appl. Phys.* **2018**, *123* (2), 025102.

https://doi.org/10.1063/1.5010237.

(40) Chen, X. J.; Hwang, J. S.; Perillat-Merceroz, G.; Landis, S.; Martin, B.; Le Si Dang, D.; Eymery, J.; Durand, C. Wafer-Scale Selective Area Growth of GaN Hexagonal Prismatic Nanostructures on c-Sapphire Substrate. *J. Cryst. Growth* **2011**, *322* (1), 15–22. https://doi.org/10.1016/j.jcrysgro.2011.03.007.

(41) Bai, J.; Dudley, M.; Chen, L.; Skromme, B. J.; Wagner, B.; Davis, R. F.; Chowdhury, U.; Dupuis, R. D. Structural Defects and Luminescence Features in Heteroepitaxial GaN Grown on On-Axis and Misoriented Substrates. *J. Appl. Phys.* **2005**, *97* (11), 116101. https://doi.org/10.1063/1.1914956.

(42) Mei, J.; Srinivasan, S.; Liu, R.; Ponce, F. A.; Narukawa, Y.; Mukai, T. Prismatic Stacking Faults in Epitaxially Laterally Overgrown GaN. *Appl. Phys. Lett.* **2006**, *88* (14), 141912. https://doi.org/10.1063/1.2193352.

(43) Roshko, A.; Brubaker, M. D.; Blanchard, P. T.; Bertness, K. A.; Harvey, T. E.; Geiss, R. H.; Levin, I. Comparison of Convergent Beam Electron Diffraction and Annular Bright Field Atomic Imaging for GaN Polarity Determination. *J. Mater. Res.* **2017**, *32* (5), 936–946. https://doi.org/10.1557/jmr.2016.443.

(44) Concordel, A.; Jacopin, G.; Gayral, B.; Garro, N.; Cros, A.; Rouvière, J.-L.; Daudin, B. Polarity Conversion of GaN Nanowires Grown by Plasma-Assisted Molecular Beam Epitaxy. *Appl. Phys. Lett.* **2019**, *114* (17), 172101. https://doi.org/10.1063/1.5094627.

(45) Coulon, P. M.; Mexis, M.; Teisseire, M.; Jublot, M.; Vennéguès, P.; Leroux, M.; Zuniga-Perez, J. Dual-Polarity GaN Micropillars Grown by Metalorganic Vapour Phase Epitaxy: Cross-Correlation between Structural and Optical Properties. *J. Appl. Phys.* **2014**, *115* (15), 153504. https://doi.org/10.1063/1.4870950.

(46) Salomon, D.; Messanvi, A.; Eymery, J.; Martínez-Criado, G. Silane-Induced N-Polarity in Wires Probed by a Synchrotron Nanobeam. *Nano Lett.* **2017**, *17* (2), 946–952. https://doi.org/10.1021/acs.nanolett.6b04291.

(47) Chen, X. J.; Perillat-Merceroz, G.; Sam-Giao, D.; Durand, C.; Eymery, J. Homoepitaxial Growth of Catalyst-Free GaN Wires on N-Polar Substrates. *Appl. Phys. Lett.* **2010**, *97* (15), 151909. https://doi.org/10.1063/1.3497078.

For Table of Contents Only

Selective area growth of GaN µ-platelets on graphene

Jonathan Henriques [1], Dyhia Tamsaout[2], Ludovic Largeau[2], Edmond Cambril[2], Lucie Valera[1,3], Gwénolé Jacopin[3], Maria Tchernycheva[2], Jean-Christophe Harmand[2], Joël Eymery[4], Christophe Durand[1*]*

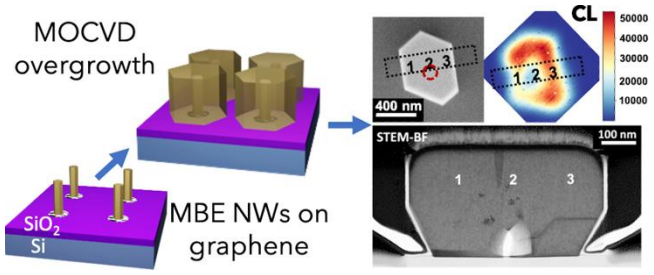

Synopsis

N-polar GaN µ-platelets selectively grown on graphene using GaN nanowire seeds on patterned arrays. Optical and structural qualities are analysed by cathodoluminescence and transmission electron microscopy, highlighting varied coalescence mechanisms and defect formation in µ-platelet growth.